A&A 553, A74 (2013)
DOI: 10.1051/0004-6361/201220659

Astronomy & Astrophysics

Properties of young star cluster systems: the age signature from near-infrared integrated colours

J. F. C. Santos Jr.[1], H. Dottori[2], and P. Grosbøl[3]

[1] Instituto de Ciências Exatas, Univ. Federal de Minas Gerais, Av. Antônio Carlos 6627, 31270-901 Belo Horizonte, MG, Brazil
e-mail: jsantos@fisica.ufmg.br
[2] Instituto de Física, Univ. Federal do Rio Grande do Sul, Av. Bento Gonçalves 9500, 91501-970 Porto Alegre, RS, Brazil
e-mail: dottori@ufrgs.br
[3] European Southern Observatory, Karl-Scharzschild-Str. 2, 85748 Garching, Germany
e-mail: pgrosbol@eso.org

Received 29 October 2012 / Accepted 29 March 2013

ABSTRACT

Context. A recent JHK_s study of several grand-design spiral galaxies, including NGC 2997, shows a bimodal distribution of their system of star clusters and star forming complexes in colour-magnitude and colour-colour diagrams. In a comparison with stellar population models including gas, the $(J - H)$ vs. $(H - K_s)$ diagram reveals that embedded clusters, still immersed in their parental clouds of gas and dust, generally have a redder $(H - K_s)$ colour than older clusters, whose gas and dust have already been ejected. This bimodal behaviour is also evident in the colour-magnitude diagram M_K vs. $(J - K_s)$, where the brightest clusters split into two sequences separating younger from older clusters. In addition, the reddening-free index $Q_d = (H - K_s) - 0.884\ (J - H)$ has been shown to correlate with age for the young clusters and thus provided an effective way to differentiate the embedded clusters from the older ones.

Aims. We aim to study the behaviour of these photometric indices for star cluster systems in the Local Group. In particular, we investigate the effectiveness of the Q_d index in sorting out clusters of different ages at their early evolutionary stages. In addition, the whole set of homogeneous measurements will serve as a template for analyses of the populations belonging to distant galaxies that are unresolved clusters or complexes.

Methods. Surface photometry was carried out for 2MASS images of populous clusters younger than ∼100 Myr whose ages were available. The integrated magnitude and colours were measured to a limiting radius and combined to generate the photometric diagrams. Some clusters, particularly the embedded ones, were studied for the first time using this method.

Results. The integrated magnitudes and colours extracted from the surface photometry of the most populous clusters/complexes in the Local Group show the expected bimodal distribution in the colour–colour and colour–magnitude diagrams. In particular, we confirm the index Q_d as a powerful tool for distinguishing clusters younger than about 7 Myr from older clusters.

Key words. galaxies: star clusters: general – infrared: galaxies – techniques: photometric

1. Introduction

The study of 55 clusters that present strong Br_γ emission ($Br_\gamma - K < -0.1$) in the grand-design spiral galaxy NGC 2997, observed with HAWK-I at VLT, has found a relationship between the reddening-free index Q_d and the Br_γ index (Grosbøl & Dottori 2012): $(Br_\gamma - K) = -0.48\ Q_d - 0.17$, indicating that $Q_d = (H - K) - 0.844(J - H)$ represents a good age indicator for $Q_d > 0.1$, which corresponds to ages <7 Myr according to Starburst 99 (Leitherer 1999; Vazquez & Leitherer 2005, hereafter SB99) evolutionary tracks. Population models generated with SB99 show nebular emission for the youngest clusters. The emission decreases with time abruptly around 7 Myr, depending on model parameters, as discussed in Sect. 4, where errors to this value are also set. Grosbøl et al. (2006) previously calibrated the equivalent width of Br_γ, or equivalently, the Br_γ index $(Br_\gamma - K)$, as an age indicator based on the ISAAC/VLT K-band spectra and SB99 evolutionary tracks. The Br_γ equivalent width is anticorrelated with the emitting region age, as previously modelled for other H emission lines in the visible (Dottori 1981; Alonso-Herrero et al. 1996). Grosbøl & Dottori (2012) also found that in the $(J - K)$ vs. M_K colour–magnitude diagram (CMD) of NGC 2997, the youngest clusters with $Q_d > 0.1$ concentrate around $(J-K) \approx 1.8$, with significant scatter due to variable extinction. They form a well-defined branch that is clearly separated from the bright older sources that concentrate around $(J - K) \approx 1.2$. This two-branch pattern is common to ten grand-design galaxies analysed by Grosbøl & Dottori (2012) and even for NGC 7424 whose cluster population is 3 mag fainter than that of NGC 2997, as seen in their Figs. 8, 9, and B.3. If the extinction varied only slowly with age, one would not expect a separation between the young and old branches in their diagrams. Thus, the gap suggests a sudden change in dust properties and/or distribution that lead to a rapid reduction of the extinction.

Studies of our Galaxy, the Large Magellanic Cloud (LMC), and the Small Magellanic Cloud (SMC) show that the interplay between stellar evolution and dust properties in the intracluster medium is a dynamic one: stellar clusters are born embedded within giant molecular clouds. During their formation and early evolution, they are often only visible at infrared wavelengths, since they are heavily obscured by dust (Lada & Lada 2003); moreover, the embedded cluster birthrate exceeds that of the visible open clusters by an order of magnitude (Lada & Lada 2003). The findings of Grosbøl & Dottori (2012) could help in

understanding the behaviour of the intracluster medium, which could be associated with the first supernovae explosions and stellar winds from O-type stars, when dust was expelled from the cluster environment (Bastian & Goodwin 2006; Goodwin & Bastian 2006; Lada & Lada 2003; Whitworth 1979). The increase in $(H - K_s)$ for younger clusters is also a consequence of the presence of hot stars because they ionise hydrogen, producing continuum emission and the Br_γ line, and also heat dust, both contributing to the flux in K.

We checked the capacity of the near-infrared (NIR) diagrams to differentiate clusters younger than 7 Myr from the older ones in a sample of clusters from the Milky Way, the Magellanic Clouds (MCs) and two clusters from M 31 and M 33, all of which have well-determined ages. In the next section, we present the NIR photometry of the Local Group clusters obtained from the 2MASS images. In Sect. 3, we compare our multi-diaphragm photometry of LMC+SMC clusters with that of Pessev et al. (2006, hereafter P06). The age limit estimate and the NIR colour sensitivity on parameters/ingredients of stellar populations evolution models are presented in Sect. 4. In Sect. 5, we discuss the observational diagnostic diagrams. In Sect. 6, we show how the Q_d index can be used as an age diagnostic tool. In Sect. 7, we discuss the results and in Sect. 8, we present our conclusions.

2. Near-infrared surface photometry of populous young star clusters

The sample listed in Table 1 is based on the selection by Portegies Zwart et al. (2010), complemented with the Milky Way embedded clusters RCW 38, NGC 3576 and M 17, which have masses higher than 500 $M_\odot$ (Lada & Lada 2003), and the LMC clusters NGC 1805, 1984, 2011, 2156, 2159 and 2172, which were studied by P06. Portegies Zwart et al. (2010) restricted their sample to well-studied populous clusters with known ages; in addition to the MCs and Milky Way clusters, NGC 604 in M 33 and vdb 0 in M 31 were also analysed. All clusters have ages up to 100 Myr. Such a sample was considered suitable to derive the integrated light properties using 2MASS mosaic images built from relatively shallow exposures. The coordinates, age, mass, reddening and distance adopted for each cluster are given in Table 1.

The JHK_s images of the 42 star clusters were downloaded from the 2MASS database using the software Montage[1], which assembles single images (512 × 1024 pix; 1″/pix) into custom mosaics preserving the spatial and calibration fidelity of the input images. A zeropoint keyword determined by the average of zeropoints provided in all single images was appended to each mosaic file for each band. Typically, the mosaics cover sky areas from 2° × 2° to 12′ × 12′ depending on the cluster size.

The clusters' centres were determined visually in the images, and the surface brightness was evaluated in the annular regions around this centre. Fixed width annuli were employed for each cluster, but they varied from 2″ to 10″ depending on the cluster size. The sky background ($F_{bg} \pm \sigma_{bg}$, in DN/pix) was determined for each band using the whole mosaiced frame by means of an algorithm that evaluates the mode of the sky distribution and rejects pixels contaminated by stars.

The cluster integrated colours and their uncertainties, the adopted aperture radius and the calculated absolute K magnitude are given in Table 1. Figure 1 shows the distribution of the absolute K magnitude with age for the Local Group clusters, characterising the sample in terms of intrinsec properties.

[1] Montage v3.3 is available in the NASA/IPAC Infrared Science Archive (http://irsa.ipac.caltech.edu/applications/2MASS/).

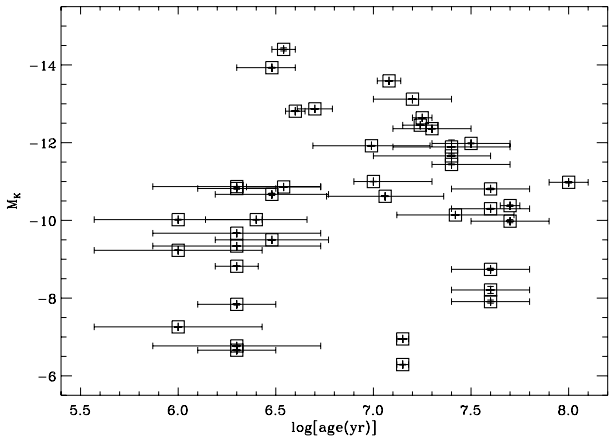

Fig. 1. Absolute K magnitude versus age for the Local Group clusters in our sample.

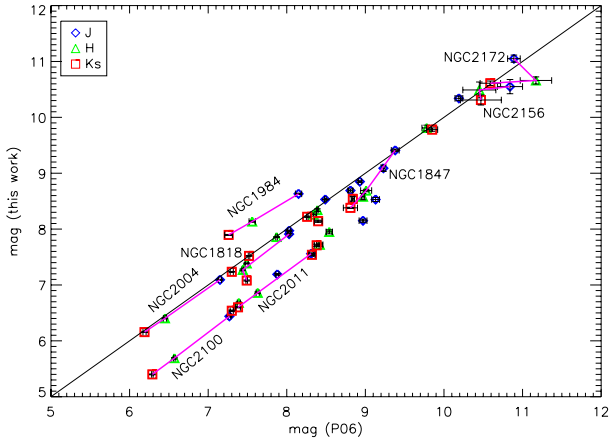

Fig. 2. Comparison of our integrated NIR magnitudes of MC clusters with those from P06. J, H and K_s magnitudes are plotted as different symbols and colours. The straight continuous line is a one-to-one relation. Line segments connect the three magnitudes for exemplary clusters.

3. Comparison: this work vs. Pessev et al. (2006)

Figure 2 shows the measured JHK_s integrated magnitudes of MCs' star clusters in common with those in the P06 sample. In the present study, we defined the area covered by a cluster as limited by the radius for which the magnitude difference from consecutive diaphragms is approximately the same as the magnitude error. The photometry performed by P06, although also based on 2MASS images, followed a different approach: both the PSF photometry (for the resolved component) and the surface photometry (for the unresolved component) were employed, and probable non-members were excluded from the final set of aperture measurements. The procedure carried out by P06 to exclude probable non-member bright stars from the integrated photometry was based on a comparison between the individual stars magnitudes derived from PSF photometry and their expected locii in a CMD considering the cluster age. Discrepancies between them indicated a probable non-member, which was then subtracted from the cluster integrated light. In our measurements, we did not exclude any star because our intention was to compare the clusters' integrated light with those obtained for

Table 1. Astrophysical parameters and integrated photometry of Local Group clusters.

Cluster/Galaxy	α_{2000} (h:m:s)	δ_{2000} (° : ′ : ″)	log [t(yr)]	log [$\mathcal{M}(M_\odot)$]	$E(B-V)$	d (kpc)	R (″)	K_s	σ_{K_s}	M_K	$J-K_s$	σ_{J-K_s}	$J-H$	σ_{J-H}	$H-K_s$	σ_{H-K_s}
NGC 869/MW	2:19:04	57:08:06	7.15 ± 0.03 (1)	4.20 (18)	0.58 (20)	2.3 (20)	100	5.06	0.01	–6.95	0.10	0.01	–0.14	0.01	0.24	0.01
NGC 884/MW	2:20:54	57:08:43	7.15 ± 0.03 (1)	4.10 (18)	0.56 (20)	2.3 (20)	140	5.71	0.01	–6.29	0.22	0.01	0.10	0.01	0.11	0.01
IC 1805/MW	2:32:43	61:27:24	6.30 ± 0.20 (2)	4.20 (18)	0.82 (20)	1.9 (20)	600	3.84	0.02	–7.84	0.71	0.02	0.49	0.02	0.23	0.02
M 42/MW	5:35:16	–5:23:15	6.00 ± 0.43 (3)	3.65 (18)	0.05 (20)	0.4 (20)	900	0.77	0.01	–7.26	1.23	0.01	0.26	0.01	0.97	0.01
NGC 2244/MW	6:31:55	4:56:36	6.30 ± 0.20 (2)	3.90 (18)	0.46 (20)	1.5 (20)	450	4.38	0.02	–6.66	0.54	0.02	0.27	0.02	0.27	0.02
RCW 38/MW	8:57:02	–47:30:41	6.00 ± 0.43 (4)	2.86 (19)	3.2 (21)	1.7 (21)	400	3.03	0.01	–9.23	2.08	0.01	1.00	0.01	1.08	0.01
Westerlund 2/MW	10:24:02	–57:45:29	6.30 ± 0.11 (2)	4.00 (18)	0.79 (20)	1.9 (20)	400	2.85	0.01	–8.82	1.62	0.01	0.80	0.01	0.82	0.01
Trumpler 14/MW	10:43:57	–59:32:49	6.30 ± 0.43 (5)	4.00 (18)	0.52 (20)	2.7 (20)	350	2.99	0.01	–9.34	1.03	0.01	0.46	0.01	0.57	0.01
NGC 3576/MW	11:11:54	–61:18:23	6.00 ± 0.43 (6)	2.86 (19)	3.5 (6)	2.6 (6)	380	3.27	0.01	–10.02	1.76	0.02	0.86	0.02	0.90	0.02
NGC 3603/MW	11:15:07	–61:15:36	6.30 ± 0.43 (7)	4.10 (18)	1.34 (20)	3.6 (20)	370	2.38	0.01	–10.87	1.51	0.01	0.71	0.01	0.79	0.01
Westerlund 1/MW	16:47:04	–45:50:38	6.70 ± 0.09 (8)	4.50 (18)	3.0 (20)	5.2 (20)	160	1.76	0.01	–12.87	1.61	0.01	0.84	0.01	0.77	0.01
[DBS2003] 179/MW	17:11:32	–39:10:47	6.54 ± 0.19 (2)	3.80 (18)	5.3 (22)	7.9 (22)	60	5.47	0.01	–10.86	2.10	0.01	1.36	0.02	0.74	0.01
Arches/MW	17:40:50	–28:49:19	6.30 ± 0.20 (9)	4.30 (18)	8.1 (23)	7.6 (23)	20	6.40	0.02	–10.82	4.35	0.04	2.61	0.04	1.74	0.04
Quintuplet/MW	17:46:15	–28:49:39	6.60 ± 0.05 (9)	4.00 (18)	8.9 (24)	8.0 (24)	30	4.80	0.01	–12.81	4.89	0.02	2.94	0.02	1.95	0.02
NGC 6611/MW	18:18:40	–13:46:42	6.48 ± 0.29 (2)	4.40 (18)	0.78 (20)	1.8 (20)	530	2.05	0.01	–9.50	1.94	0.02	1.07	0.02	0.87	0.02
M 17/MW	18:20:30	–16:10:45	6.30 ± 0.43 (10)	2.95 (19)	1.51 (20)	1.3 (20)	450	1.42	0.01	–9.67	1.91	0.01	0.83	0.01	1.07	0.02
RSGC 01/MW	18:37:58	–6:53:00	7.08 ± 0.06 (11)	4.50 (18)	7.9 (25)	5.8 (25)	130	2.97	0.01	–13.59	3.71	0.01	2.43	0.01	1.28	0.01
RSGC 02/MW	18:39:20	–6:01:42	7.24 ± 0.09 (11)	4.60 (18)	4.2 (26)	5.8 (26)	130	2.83	0.01	–12.45	2.05	0.01	1.13	0.01	0.93	0.01
RSGC 03/MW	18:46:19	–3:23:16	7.25 ± 0.05 (12)	4.50 (18)	4.2 (12)	6.0 (12)	200	2.71	0.01	–12.64	2.46	0.01	1.52	0.01	0.94	0.01
Cyg OB 2/MW	20:33:15	41:18:50	6.40 ± 0.26 (2)	4.40 (18)	2.9 (27)	1.7 (27)	440	2.14	0.01	–10.02	1.04	0.01	0.60	0.01	0.44	0.01
NGC 7380/MW	22:47:15	58:06:34	6.30 ± 0.43 (2)	3.80 (18)	0.60 (20)	2.2 (20)	300	5.15	0.02	–6.77	0.93	0.02	0.58	0.02	0.35	0.02
NGC 330/SMC	0:56:19	–72:27:49	$7.40^{+0.20}_{-0.40}$ (13)	4.56 (18)	0.03 (28)	60.0 (28)	60	7.24	0.01	–11.66	0.74	0.01	0.59	0.01	0.15	0.01
NGC 346/SMC	0:59:05	–72:10:40	6.48 ± 0.29 (14)	5.60 (18)	0.03 (28)	60.0 (28)	90	8.23	0.03	–10.67	0.63	0.03	0.17	0.03	0.46	0.04
NGC 1711/LMC	4:50:37	–69:59:00	7.70 ± 0.05 (15)	4.24 (18)	0.07 (28)	50.0 (28)	70	8.14	0.02	–10.38	0.55	0.02	0.43	0.01	0.12	0.02
NGC 1805/LMC	5:02:22	–66:06:45	$7.00^{+0.30}_{-0.10}$ (15)	3.52 (15)	0.07 (28)	50.0 (28)	50	7.52	0.01	–11.00	1.01	0.01	0.67	0.01	0.34	0.01
NGC 1818/LMC	5:04:14	–66:26:02	$7.40^{+0.30}_{-0.10}$ (15)	4.42 (18)	0.07 (28)	50.0 (28)	90	7.08	0.01	–11.44	0.83	0.01	0.63	0.01	0.19	0.01
NGC 1847/LMC	5:07:08	–68:58:23	7.42 ± 0.30 (15)	4.44 (18)	0.07 (28)	50.0 (28)	40	8.38	0.01	–10.14	1.03	0.02	0.72	0.02	0.31	0.02
NGC 1850/LMC	5:08:45	–68:45:41	7.50 ± 0.20 (15)	4.86 (18)	0.07 (28)	50.0 (28)	110	6.54	0.01	–11.98	0.65	0.01	0.52	0.01	0.14	0.01
NGC 1984/LMC	5:27:40	–69:08:06	7.06 ± 0.30 (15)	3.38 (15)	0.07 (28)	50.0 (28)	40	7.90	0.01	–10.62	0.74	0.01	0.49	0.01	0.24	0.01
NGC 2004/LMC	5:30:40	–67:17:14	7.30 ± 0.20 (15)	4.36 (18)	0.07 (28)	50.0 (28)	100	6.16	0.01	–12.36	0.94	0.01	0.69	0.01	0.25	0.01
NGC 2011/LMC	5:32:19	–67:31:18	6.99 ± 0.30 (15)	3.47 (15)	0.07 (28)	50.0 (28)	110	6.60	0.01	–11.92	0.96	0.01	0.70	0.01	0.26	0.01
NGC 2070/LMC	5:38:42	–69:06:03	$6.48^{+0.12}_{-0.18}$ (15)	4.78 (18)	0.07 (28)	50.0 (28)	270	4.59	0.01	–13.93	0.84	0.01	0.31	0.01	0.53	0.01
NGC 2100/LMC	5:42:08	–69:12:38	7.20 ± 0.20 (15)	4.36 (18)	0.07 (28)	50.0 (28)	170	5.40	0.01	–13.12	1.04	0.01	0.75	0.01	0.29	0.01
NGC 2136/LMC	5:52:58	–69:29:30	8.00 ± 0.10 (15)	4.30 (18)	0.07 (28)	50.0 (28)	100	7.54	0.02	–10.98	0.61	0.02	0.42	0.02	0.18	0.02
NGC 2157/LMC	5:57:35	–69:11:46	7.60 ± 0.20 (15)	4.31 (18)	0.07 (28)	50.0 (28)	60	8.22	0.01	–10.30	0.63	0.01	0.52	0.01	0.12	0.02

Table 1. continued.

Cluster/Galaxy	α_{2000} (h:m:s)	δ_{2000} (° : ′ : ″)	log [t(yr)]	log [$\mathcal{M}(M_\odot)$]	$E(B-V)$	d (kpc)	R (″)	K_s	σ_{K_s}	M_K	$J-K_s$	σ_{J-K_s}	$J-H$	σ_{J-H}	$H-K_s$	σ_{H-K_s}
NGC 2156/LMC	5:57:50	–68:27:38	7.60 ± 0.20 (15)	3.63 (15)	0.07 (28)	50.0 (28)	60	10.31	0.09	–8.21	0.24	0.09	0.07	0.07	0.18	0.11
NGC 2159/LMC	5:58:03	–68:37:22	7.60 ± 0.20 (15)	3.65 (15)	0.07 (28)	50.0 (28)	40	9.78	0.03	–8.74	0.56	0.03	0.53	0.02	0.03	0.04
NGC 2164/LMC	5:58:55	–68:30:57	7.70 ± 0.20 (15)	4.18 (18)	0.07 (28)	50.0 (28)	90	8.54	0.04	–9.98	0.55	0.04	0.50	0.03	0.04	0.04
NGC 2172/LMC	6:00:05	–68:38:13	7.60 ± 0.20 (15)	3.52 (15)	0.07 (28)	50.0 (28)	30	10.61	0.04	–7.91	0.44	0.05	0.39	0.03	0.05	0.05
NGC 2214/LMC	6:12:58	–68:15:36	7.60 ± 0.20 (15)	4.03 (18)	0.07 (28)	50.0 (28)	110	7.71	0.02	–10.81	0.82	0.03	0.57	0.02	0.24	0.03
VdB 0/M 31	0:40:29	40:36:15	7.40 ± 0.30 (16)	4.85 (18)	0.05 (28)	783.0 (28)	20	12.65	0.18	–11.89	0.46	0.19	0.46	0.14	0.00	0.22
NGC 604/M 33	1:34:33	30:47:00	6.54 ± 0.06 (17)	5.00 (18)	0.04 (28)	883.0 (28)	40	10.34	0.04	–14.40	1.16	0.05	0.44	0.06	0.72	0.07

Notes. Literature sources for age, photometric mass, reddening and distance are indicated within parentheses.

References. (1) Currie et al. (2010); (2) Pfalzner (2009); (3) Hillenbrand & Hartmann (1998); (4) Wolk et al. (2006); (5) Ascenso et al. (2007); (6) Figueredo et al. (2002); (7) Harayama et al. (2008); (8) Mengel & Tacconi-Garman (2007); (9) Figer et al. (1999); (10) Povich et al. (2009); (11) Figer (2008); (12) Clark et al. (2009); (13) Mackey & Gilmore (2003b); (14) Sabbi et al. (2008); (15) Mackey & Gilmore (2003a); (16) Perina et al. (2009); (17) Maíz-Apellániz (2001); (18) Portegies Zwart et al. (2010); (19) Lada & Lada (2003); (20) WEBDA (http://www.univie.ac.at/webda/); (21) Smith et al. (1999); (22) Borissova et al. (2008); (23) Martins et al. (2008); (24) Liermann et al. (2012); (25) Figer et al. (2006); (26) Davies et al. (2007); (27) Knödlseder (2000); (28) NED/NASA (http://ned.ipac.caltech.edu/).

Fig. 3. Comparison of our integrated NIR colours of MC clusters with those from P06. $(J-H)$ and $(J-K_s)$ colours are plotted as blue diamonds and red squares, respectively. The straight continuous line is a one-to-one relationship. Line segments connect colours of cluster outliers.

clusters/complexes observed in distant galaxies. While P06 included different error sources, even the error introduced by background stochastic fluctuations, in the present analysis, only the photometric errors were considered. To quantify these errors, we used for each band the total noise variance as given in the Explanatory Supplement to the 2MASS All Sky Data Release[2], i.e., $\sigma_{\rm band} = \sqrt{n \times \sigma_{\rm bg}^2 \times [(4 \times 1.7^2) + 1.8 \times 10^{-3} n]}$, where n is the number of pixels in the aperture and $\sigma_{\rm bg}$ is the measured background noise (in DN/pix). The magnitude error in a given aperture was then obtained by $\sigma_{\rm mag} = 1.0857 \times \sigma_{\rm band}/F_{\rm band}$, where $F_{\rm band}$ is the background subtracted flux in DN. The calibrated integrated magnitude in each band was $mag_{\rm cal} = zeropoint - 2.5 \log F_{\rm band}$. The colour errors were determined by propagating the integrated magnitude errors from the relevant bands. Because P06 yields integrated magnitudes for several diaphragms, we selected the one that matches our adopted limiting radius for the following analysis.

The integrated magnitudes comparison is shown in Fig. 2. There is a general agreement between both studies for all three bands. The continuous line is a one-to-one relation. Some clusters, taken as examples to illustrate the colours behaviour, are indicated by line segments connecting the three bands. Line segments parallel to the one-to-one relation reveal clusters that have identical colours in P06 and our study. Crooked or slanted line segments yield different colours in P06 and our study. The colours comparison is shown in Fig. 3 and indicates clusters with dissimilar colours compared to those from P06.

The effect of the different adopted centres and background corrections were investigated for these clusters to search for an explanation for the discrepancies found. Figure 4 presents the results of the changing centre and the background correction for the aforementioned clusters on the $(J-H)$ vs. $(H-K_s)$ diagram. The adopted cluster centre plus four positions shifted from this centre by 10″ towards the E, W, N and S, respectively, were considered, and the colours were determined for each of centre. The sky estimates were evaluated in five different fields, defined as square areas of a typical size 2 times larger than the cluster adopted limit (see Table 1), and the colours determined for the clusters maintained their original adopted centres. The colours derived from the original sky estimate using the whole mosaiced

[2] http://www.ipac.caltech.edu/2mass/releases/allsky/doc/sec6_8a.html

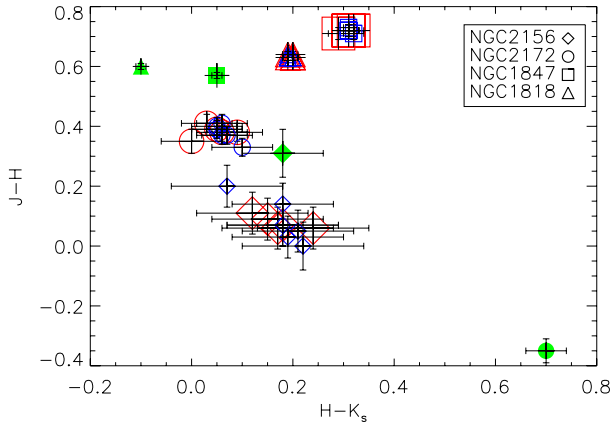

Fig. 4. Colour–colour diagram of the outlier clusters indicated in Fig. 3. P06 measurements are indicated by filled green symbols. Large open red symbols represent the effect of adopting different cluster centres. Small open blue symbols show the effect of different sky backgrounds.

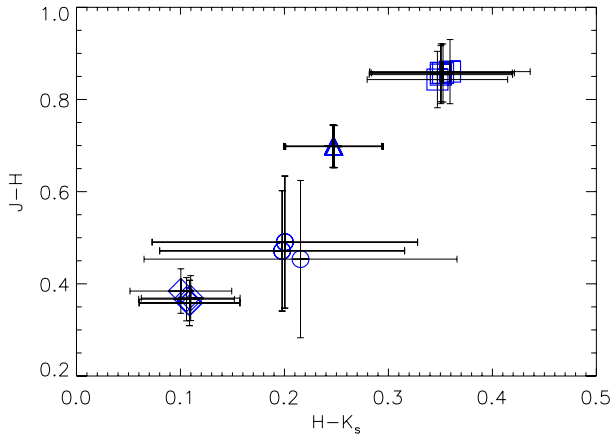

Fig. 5. Colour–colour diagram of the outlier clusters indicated in Fig. 4 based on the integrated flux of individual stars within the adopted cluster limit. The symbols are the same as in Fig. 4. The influence of the different centres is shown for each cluster.

frame is also plotted, as well as the colours from P06 for these four clusters, where we plotted their colours for the diaphragm that matches our adopted cluster limit. The effect of the moderate centre shifts and the different sky corrections appear not to account for the discrepancy of the cluster colours in comparison with the P06 measurements. Particularly, NGC 2172 presents a huge difference in both colours. NGC 2156, on the other hand, in spite the larger photometric errors, present colours compatible with P06. NGC 1818 and NGC 1847 have a disagreement in $(H - K_s)$.

Figure 5 shows the $(J-H)$ vs. $(H-K_s)$ diagram for the same clusters but with integrated colours calculated from the 2MASS point source catalogue (PSC); i.e., the individual star flux for all stars within the adopted cluster limit was added up. The colours resulting from the different centring (10″ shifts) were also plotted. The different centres do not affect the cluster colours significantly. Because P06 did not provide a list of members and the star distribution in the NIR CMDs of these clusters does not define well the expected evolutionary sequences, we did not attempt to subtract the integrated flux from the flux of the possible non-members, which prevented us of making a direct comparison with the P06 photometry.

It is worth noticing, however, that the four clusters mentioned with colour discrepancies have no apparent sign of gas.

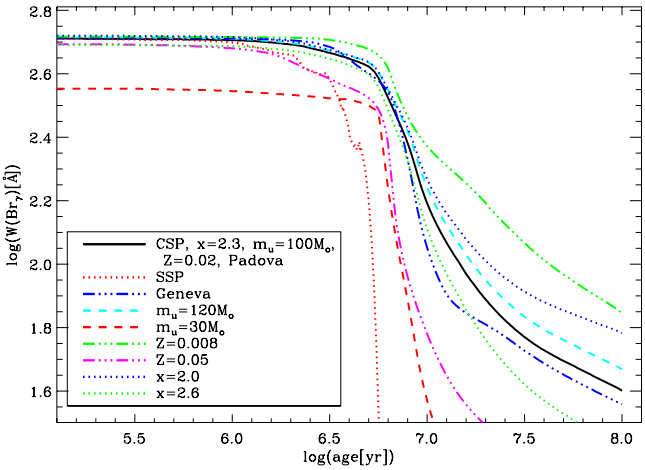

Fig. 6. Equivalent width of Br$_\gamma$ as a function of age according to SB99 models. The base model parameters/input are defined by continuous star formation (CSP), Kroupa IMF with upper mass $m_u = 100\,M_\odot$, metallicity $Z = 0.02$ and Padova tracks (continuous black line). In the following models, all parameters/input of the base model are kept, except for one variable replacement: simple stellar populations (SSP) (dotted red line); Geneva tracks (dot-dashed blue line); upper mass $m_u = 120\,M_\odot$ (dashed cyan line); upper mass $m_u = 30\,M_\odot$ (dashed red line); metallicity $Z = 0.008$ (dot-dashed green line); metallicity $Z = 0.05$ (dot-dashed magenta line); Kroupa IMF with upper slope $x = 2.0$ (dotted blue line); Kroupa IMF with upper slope $x = 2.6$ (dotted green line).

We searched for stars that could be responsible for the colour differences. In accord to Worthey & Lee (2011) and Straizys & Lazauskaitė (2009) there are no stars with colours blue enough to produce a $(J - H)$ colour like that of NGC 2172 quoted by P06. Our integrated colours calculated from surface photometry (Fig. 4) and individual star fluxes (Fig. 5) agree, but diverge from that of P06. As NGC 2172 colours would fall in a rather peculiar position in the colour–colour diagram and not being fit by any model (see Fig. 9), this indicates that P06 photometry may be incorrect for NGC 2172. Because the differences between our photometry of NGC 1818 and NGC 1847 and that of P06 are not as large as for NGC 2172, their colour discrepancies may be explained by the exclusion of bright non-member star(s) in P06 photometry. NGC 2156 has a smaller colour discrepancy which also can be attributed to non-member star(s) being removed in P06 photometry but not in ours photometry.

4. Evolution of stellar populations NIR colours: model predictions

On theorethical grounds, it can be demonstrated that the drop of Br$_\gamma$ emission, associated with the evolution of hot stars that are not capable anymore of ionising the gas in the intracluster medium, occurs at an age of ~7 Myr. With this aim, Fig. 6 presents the behaviour of the Br$_\gamma$ equivalent width with the age according to SB99 models (v6.0.4). We used as base model the one with continuous star formation population (CSP), standard Kroupa (2001) IMF ($x = 2.3$ for masses above $0.5\,M_\odot$ and $x = 1.3$ for masses below $0.5\,M_\odot$) with upper stellar mass $m_u = 100\,M_\odot$, solar metallicity ($Z = 0.02$) and Padova (Bertelli et al. 1994; Girardi et al. 2000) stellar evolutionary tracks. Other models for which one parameter or ingredient is changed in the base model are represented in Fig. 6. The whole set of models entails the effect of several variables on the age at which the

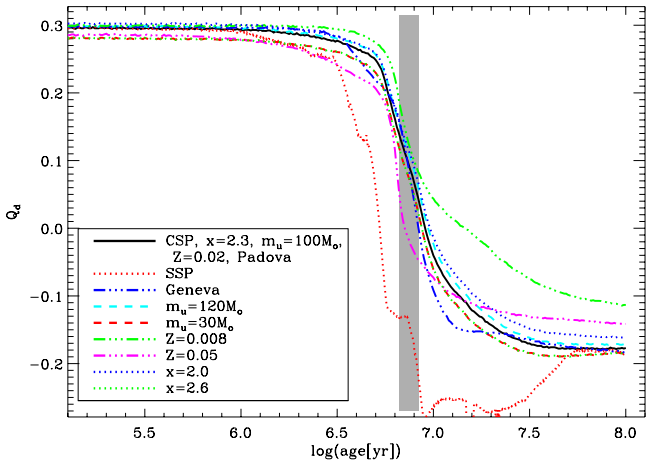

Fig. 7. Reddening-free parameter as a function of age according to SB99 models. The model parameters/input are defined as in Fig. 6. The grey area represents the age (and uncertainty) estimate for the evolutionary transition between young clusters with nebular emission and older clusters without nebular emission.

Br_γ drops, according to SB99 models. We explored a range of properties that represent a realistic approach to our problem.

Based on the models considered in Fig. 6, we computed, for each model, the age at which the Br_γ equivalent width falls by half of its maximum value. Then the average age and its standard deviation were estimated as 7.5 ± 0.9 Myr and considered as the age limit separating younger populations with nebular emission from older populations without nebular emission.

SB99 models also allowed us to investigate the behaviour of the reddening-free index Q_d with age and its sensitivity to the aforementioned parameters (Fig. 7). The age limit and its uncertainty as calculated above was used as a constraint for the range of Q_d representing the transition between young and old clusters. The higher density of models intersecting the age transition region lies around $Q_d = 0.1$, consistent with Grosbøl & Dottori (2012) findings. However, as a cautionary note, it can be seen that in this region Q_d as low as −0.15 or as high as +0.15 are accessible to specific models. Lower values of Q_d favour the base model with the SSP instead of CSP as the star formation mode and a low upper stellar mass. Higher values of Q_d favour the base model (CSP, $m_u = 100\,M_\odot$).

Aiming at a comparison with the observations, the parameter space covered by different models was further investigated in the $(J-H)$ vs. $(H-K_s)$ diagram (Fig. 8). SSP models by Maraston (2005, hereafter M05) are shown for metallicities $Z = 0.009$, 0.05 and 0.02 (solar) and a Kroupa (2001) IMF and compared to SSPs built with updated Padova tracks (Marigo et al. 2008) for the same metallicities (Fig. 8a). These models do not include nebular emission. Bastian et al. (2006) showed that the M05 models would fit complexes in the Antennae (after reddening correction) better than SB99 models, which they attribute to the different treatment of the red supergiant phase. We found that Padova SSPs show a trend with metallicity opposite to those of M05 SSPs (see the solar and above solar paths in Fig. 8a) but none of them reach extreme red colours. In any case, M05 models do produce redder colours for the oldest SSPs compared to Padova SSPs, but their SSP colours are similar for populations younger than 7 Myr. Figure 8b presents the effect of nebular emission on Padova SSP colours. Our base SB99 model, i.e., CSPs built with Padova tracks, solar metallicity, Kroupa's IMF with stellar mass upper limit $100\,M_\odot$ and nebular emission is compared to that without nebular emission in Fig. 8c. Clearly the effect of nebular emission is to increase $(H-K_s)$ and $(J-H)$ for younger populations. We also investigated the base model colour sensitivity to the upper mass limit (Fig. 8d), to the metallicity (Fig. 8e), and to the IMF slope above $0.5\,M_\odot$ (Fig. 8f). $(H-K_s)$ increases for the younger populations when the upper mass limit increases, the metallicity decreases and the IMF slope decreases. For the range of parameters considered, the IMF slope seems to have the smaller effect on the colours, but they are strongly affected by the upper mass limit. In general, plausible variations of the parameters/ingredients investigated are not capable of matching all Local Group cluster colours without dust extinction (see next section).

5. Local Group clusters: the age effect on infrared colour indices

Our sample is characterised in Figs. 9 and 10, where the measured NIR fluxes for the 42 clusters are complemented by the ages found in the literature (see Table 1). The age provided come from CMD fittings of isochrones derived from different stellar evolutionary models and the quoted uncertainties from the literature (large in most cases) should account for discrepancies resulting from the use of the different methods of age determination, minimising the effect of their heterogeneity. We detected an error in the age quoted by Portegies Zwart et al. (2010) for Westerlund 1, that should be 5 Myr instead of 3.5 Myr.

The observed colour–colour diagram (Fig. 9) corroborates the explanation provided by Grosbøl & Dottori (2012) for the distribution of the clusters in grand-design spiral galaxies. The clusters can be separated into two main regions in the diagram. The redder group is younger than 7 Myr and associated with high extinction, and the bluer group is older and associated with relatively low extinction. Figure 9 clearly shows that our sample of clusters younger than 7 Myr fills regions of high extinction that are not reached by their older counterparts.

In Fig. 9, the colours of the Padova single-burst stellar populations (SSP) with ages between 1 Myr and 100 Myr and the SB99 CSP with ages between ≈0 Myr and 100 Myr are shown. Dust and nebular emission are included in the SB99 models. Both models were built using as ingredients a standard Kroupa's IMF and solar metallicity. The different extinction models are indicated for a visual extinction of $A_V = 5$. The standard reddening vector, the so-called *screen* model, accounts for the foreground extinction (Indebetouw et al. 2005), while the reddening vector characterised by the *dusty* model accounts for intracluster dust, where the dust and stars are mixed (Israel et al. 1998; Witt et al. 1992). The observed colours of the reddest cluster in our sample, Quintuplet, were connected to the colours of the SB99 CSP, with an age of 4 Myr, the cluster age (see Table 1). Quintplets' extinction corresponds to $A_V \approx 16$ and closely follows the *screen* dust model, as observed by comparing the cluster extinction slope with that of the extinction models. A similar argument applied to the other two clusters close to the Galactic centre, Arches and [DBS2003] 179, leads to the same conclusion: because they are younger than 7 Myr, linking their observed colours to their intrinsic colours (CSP models between 0 Myr and 10 Myr) yields extinction vector slopes more akin to the *screen* model than to the *dusty* model.

Many clusters are compatible with both the screen and dusty models. The SB99 CSP models were generated with a stellar upper mass limit of $m_u = 100\,M_\odot$, which, in the colour–colour diagram, are suitable for reproducing the colours for most

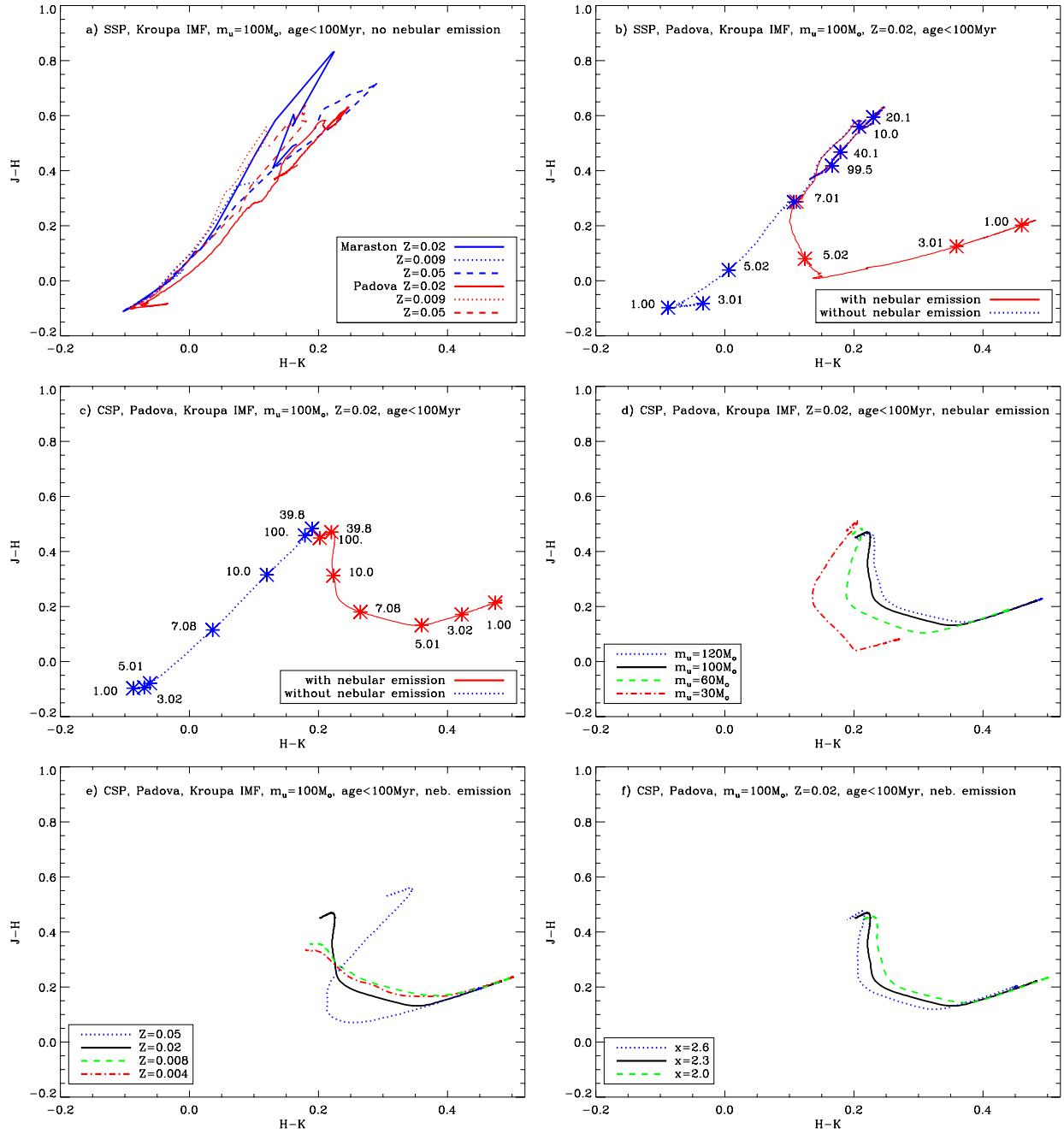

Fig. 8. Colour evolution of stellar populations up to 100 Myr according to different models and ingredients. Fixed parameters are indicated at the top while variable ones at the bottom. **a)** Comparison between SSPs built with Padova tracks and SSPs from Maraston (2005) for different metallicities. **b)** SSPs with Padova tracks including nebular emission compared to those without nebular emission. **c)** Same as in **b)** for CSPs. **d)** CSP models built with a Kroupa IMF and variable upper stellar mass limit. **e)** CSP models built with different metallicities. **f)** CSP models built with different slopes for the IMF above 0.5 $M_{\odot}$. Age (Myr) is indicated at selected evolutionary stages in panels **b)** and **c)**.

of the sample. NGC 889, NGC 864 and NGC 2156 are better characterised by models with $m_{\rm u} = 20{-}30\,M_{\odot}$ and a low extinction, while M 42 is only characterised by a young population (0–2 Myr), but its colours are uncompatible with normal extinction.

The distribution of the clusters in the $(J-K)$ vs. M_K CMD, together with the $Q_{\rm d}$ vs. M_K diagram, is shown in Fig. 10, where the grey rectangle indicates values of $Q_{\rm d}$ corresponding to the transition between young and old clusters. Note that the most probable value is $Q_{\rm d} = 0.1$ and its distribution is not symmetric around that value. For the $(J-H)$ vs. $(H-K_{\rm s})$ diagram, Fig. 10 reveals that most of the youngest clusters (blue circles) have a tendency to be located in specific regions of both diagrams. In particular, 10 out of 19 clusters with ages less than 7 Myr have a reddening-free index of $Q_{\rm d} > 0.1$. This proportion does not change if we use 7.5 Myr as the age limit. The three very young bright clusters with $Q_{\rm d} < -0.3$, Arches, Quintuplet and [DBS2003] 179, are objects close enough to the Galactic centre to have their evolution influenced by the strong tidal field, with their gas and dust already being stripped in the early phases. They appear very red because of the strong foreground extinction instead of their intracluster gas/dust content. If these clusters are disregarded, then ≈60% of the youngest clusters have a reddening-free index of $Q_{\rm d} > 0.1$.

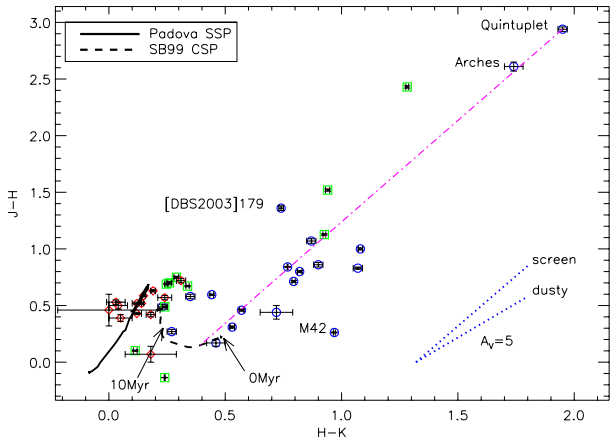

Fig. 9. Sample observed colour–colour diagram with different symbols indicating age ranges: t(Myr) < 7 (blue circle), 7 < t(Myr) < 20 (green square), 20 < t(Myr) < 100 (red diamond). The three young clusters near the Galactic centre and M 42 are labelled. Continuous and dashed lines represent the colours of the Padova SSPs and the SB99 CSP, respectively. Model ages range from very early phases to 100 Myr, indicated for the CSP models. The magenta dot-dashed line connects the observed and the intrinsic colours of Quintuplet. Blue dotted lines show the extinction yielded by $A_V = 5$ for both a standard *screen* reddening vector and a *dusty* cluster medium.

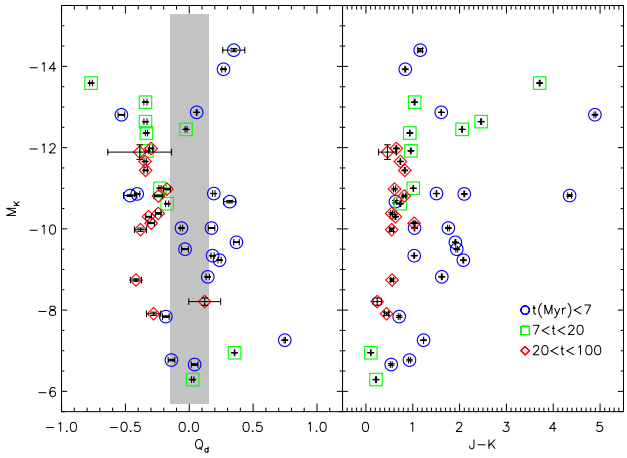

Fig. 10. *Left*: absolute K_s band magnitudes versus the reddening-free index Q_d for 42 clusters in the Local Group with ages up to 100 Myr; The grey bar indicates the range of Q_d values corresponding to the transition between young and old clusters, according to Fig. 7. *Right*: colour−magnitude diagram for the same clusters.

Because less massive clusters colours may be affected by stochastic effects arising from small numbers of bright stars, a new colour–colour diagram was built (see Fig. 11) by binning in age the cluster colours, computed from the integrated flux in *JHK* and consequently these are flux-weigthed colours. This procedure guarantees that intrinsically fainter clusters will have low weight. To compute the final colours we did not weight the individual cluster colours by their signal to noise or any other parameter. The age bin is 0.2 in log t. There is a clear separation among the binned clusters indicating two sequences in that the younger populations are redder in $(H - K_s)$.

6. Age diagnostic based on Q_d

The age distribution of clusters up to 100 Myr can be divided into clusters older (O) and younger (Y) than 7 Myr according to

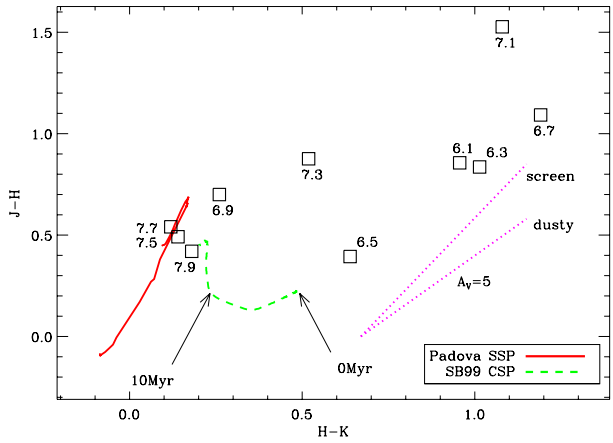

Fig. 11. Colour–colour diagram for age binned clusters with bin log t = 0.2. The age (log t) is indicated. Padova SSP and SB99 CSP models are superimposed. Dust effect according to the *dusty* and the *screen* models are represented as in Fig. 9.

$Q_d < 0.1$ and $Q_d > 0.1$, respectively. Applying this to our observed sample of Local Group clusters, for $Q_d < 0.1$, we detect 21 true old clusters (O_t) and 6 (excluding the three clusters near the Galactic centre) false old clusters (O_f), i.e., young clusters with $Q_d < 0.1$. Similarly, for $Q_d > 0.1$, we detect 10 true young clusters (Y_t) and 2 false young clusters (Y_f), i.e., old clusters with $Q_d > 0.1$. Consequently, 78% of the clusters having $Q_d < 0.1$ are true old clusters ($O_t/(O_t + O_f)$), and 22% are misclassified clusters younger than 7 Myr. In a similar way, 83% of the clusters having $Q_d > 0.1$ are true young clusters ($Y_t/(Y_t + Y_f)$), and 17% are misclassified clusters older than 7 Myr. The statistics also shows that, by using $Q_d = 0.1$ as a discriminator, we recover ≈60% ($Y_t/(Y_t + O_f)$) from the total sample of young clusters and ≈90% ($O_t/(O_t + Y_f)$) from the total sample of old clusters.

Because we selected the most massive clusters and star forming complexes of the Local Group galaxies, the sample is, on average, representative of the brightest (youngest) clusters in similar environments. Consequently, beyond the qualitative agreement of our sample NIR diagrams with those of distant galaxies (Grosbøl & Dottori 2012), the Q_d index provides a reliable quantitative measure of the proportion of clusters/complexes younger than 7 Myr in galaxies. A large fraction (83%) of the clusters with $Q_d > 0.1$ are genuinely younger than 7 Myr and a similarly large fraction (78%) of the clusters with $Q_d < 0.1$ are in the age range 7−100 Myr.

7. Discussion

Our results validate the use of the Q_d index to differentiate star clusters in their early stages of evolution. The sample employed in the present study is not complete, but by selecting the most massive clusters/complexes with available ages in the Local Group, we hope to have gathered an unbiased sample. One difference from the cluster samples in Grosbøl & Dottori (2012) is the lower cluster mass limit in our sample (≈500 $M_\odot$), which may introduce some bias due to the integrated colour scattering produced by a few heavy OB stars. Another issue is that, being lower metallicity galaxies, the MC clusters may have lower metallicity, in average, than those in the Milky Way and M 31, making the sample not completely homogeneous on this aspect.

The Q_d vs. M_K diagram (Fig. 10) clearly shows a segregation of clusters by age and led us to give an estimate of the proportion of clusters younger than 7 Myr over all clusters with $Q_d > 0.1$,

which should be expected in galaxies outside the Local Group if the processes involved in cluster formation and evolution are similar. As Fig. 10 shows, there is very little contamination of clusters older than 7 Myr among those with $Q_d > 0.1$. It is feasible to estimate the size of the population of clusters younger than 7 Myr for a distant galaxy observed in JHK_s. From the measured colours of the star clusters and the star forming regions and the calculated Q_d index, one can count the number of clusters with $Q_d > 0.1$, which are ≈60% of the total number of objects with 7 Myr. Consequently, the total number of these objects can be obtained. A similar analysis for $Q_d < 0.1$ would lead to an estimate of the population of older clusters. Because of their peculiar evolutionary characteristics, the clusters near the Galactic centre were excluded from the above statistics, and the object counts in distant galaxies should exclude those clusters too close to their centres. Nuclear clusters were also excluded in the Grosbøl & Dottori (2012) study of cluster systems in external galaxies.

We showed that the clusters near the Galactic centre in our sample, i.e., Arches, Quintuplet and [DBS2003] 179, have high extinctions associated mainly with foreground reddening (as opposed to intracluster dust), which nearly follows a standard *screen* reddening vector (Fig. 9). They are clusters younger than 7 Myr and their extreme NIR colours are a consequence of the heavy extinction towards the Galactic centre. The stellar population at these early ages cannot produce extremely red colours, as demonstrated by the locus of the evolutionary models plotted in Fig. 9.

In summary, if $Q_d > 0.1$, then 60% of the clusters must be genuinely younger than 7 Myr, with very few older clusters showing up in this region (Fig. 9). The remaining 40% of the clusters, with an index of $Q_d < 0.1$, can be explained by their association to extinctions consistent with a standard *screen* reddening vector. Such very young, dust depleted clusters, as in the cases of the three clusters near the Galactic centre in our sample, can occur as a consequence of extreme environmental conditions such as strong tidal fields.

8. Conclusions

We analysed the NIR colour indexes of 42 clusters in the Local Group with ages determined by other authors to test the capacity of the reddening-free colour index Q_d to distinguish clusters younger than 7 Myr from the older clusters. The index failed to classify 6 out of the 16 clusters younger than 7 Myr and misclassified 2 out of the 23 clusters older than 7 Myr. Because the reddening-free index verifies $Q_d > 0.1$ for a broad variety of galaxies, cluster masses and environments, we conclude that it is most likely associated more with the dust distribution with regard to the cluster stars than with the metallicity or the IMF.

The sudden change of the index is most likely linked to the expulsion of the dust from the cluster due to stellar evolution, mainly SN explosions, characterising the transition from the mix of stars and dust inside the cluster (Israel et al. 1998; Witt et al. 1992) to the screening of the starlight by external dust (Indebetouw et al. 2005). It is also related to gas and dust emission, i.e. the presence of hot stars can excite Br_γ and heat dust, which increases $(H - K_s)$ for younger clusters.

The Q_d index provides a way to distinguish very young clusters/star forming complexes up to 7 Myr old from the older clusters for galaxies observed in JHK_s. In addition, we showed that the index estimates the proportion of clusters in such age ranges.

Acknowledgements. We acknowledge the anonymous referee who has helped us to clarify and improve significantly the paper. We thank the GSFC Astronomy User's Library group and W. Landsman for the IDL program used to estimate the images sky background. This research has made use of the following databases: WEBDA, operated at the Institute for Astronomy of the University of Vienna; NASA/IPAC Extragalactic Database (NED) and NASA/IPAC Infrared Science Archive, both operated by the Jet Propulsion Laboratory, California Institute of Technology, under contract with the National Aeronautics and Space Administration. This research made use of Montage, funded by the NASA's Earth Science Technology Office, Computation Technologies Project, under Cooperative Agreement Number NCC5-626 between NASA and the California Institute of Technology. Montage is maintained by the NASA/IPAC Infrared Science Archive. The english version of this paper was revised by AJE.

References

Alonso-Herrero, A., Aragon-Salamanca, A., Zamorano, J., & Rego, M. 1996, MNRAS, 278, 417
Ascenso, J., Alves, J., Vicente, S., & Lago, M. T. V. T. 2007, A&A, 476, 199
Bastian, N., & Goodwin, S. P. 2006, MNRAS, 367, L9
Bastian, N., Emsellem, E., Kissler-Patig, M., & Maraston, C. 2006, A&A, 445, 471
Bertelli, G., Bressan, A., Chiosi, C., Fagotto, F., & Nasi, E. 1994, A&AS, 106, 275
Borissova, J., Ivanov, V. D., Hanson, M. M., et al. 2008, A&A, 488, 151
Chandar, R., Whitmore, B. C., & Fall, S. M. 2010, ApJ, 713, 1343
Clark, J. S., Negueruela, I., Davies, B., et al. 2009, A&A, 498, 109
Currie, T., Hernandez, J., & Irwin, J. 2010, ApJS, 186, 191
Davies, B., Figer D. F., Kudritzki, R. P., et al. 2007, ApJ, 671, 781
Dottori, H. A. 1981, Ap&SS, 80, 267
Figer, D. F. 2008, in Massive Stars as Cosmic Engines, eds. F. Bresolin, P. A. Crowther, & J. Puls, Proc. IAU Symp., 250, 247
Figer, D. F., McLean, I. S., & Morris, M. 1999, ApJ, 514, 202
Figer, D. F., MacKenty, J. W., Robberto, M., et al. 2006, ApJ, 643, 1166
Figueredo, E., Blum, R. D., Damineli, A., & Conti, P. S. 2002, AJ, 124, 2739
Girardi, L., Bressan, A., Bertelli, G., & Chiosi, C. 2000, A&AS, 141, 371
Goodwin, S. P., & Bastian, N. 2006, MNRAS, 373,752
Grosbøl, P., & Dottori, H. 2012, A&A, 542, A39
Grosbøl, P., Dottori, H., & Gredel, R. 2006, A&A, 453, L25
Harayama, Y., Eisenhauer, F., & Martins, F. 2008, ApJ, 675, 1319
Hillenbrand, L. A., & Hartmann, L. W. 1998, ApJ, 492, 540
Indebetouw, R., Mathis, J. S., Babler, B. L., et al. 2005, ApJ, 619, 931
Israel, F. P., van den Werf, P. P., Hawarden, T. G., & Aspin, C. 1998, A&A, 336, 433
Knödlseder, J. 2000, A&A, 360, 539
Kroupa, P. 2001, MNRAS, 322, 231
Lada, C. J., & Lada, E. A. 2003, ARA&A, 41, 57
Leitherer, C., Schaerer, D., Goldader, J. D., et al. 1999, ApJS, 123, 3
Liermann, A., Hamann, W. R., & Oskinova, L. M. 2012, A&A, 540, A14
Mackey, A. D., & Gilmore, G. F. 2003a, MNRAS, 338, 85
Mackey, A. D., & Gilmore, G. F. 2003b, MNRAS, 338, 120
Maíz-Apellániz, J. 2001, ApJ, 563, 151
Maraston, C. 2005, MNRAS, 362, 799
Marigo, P., Girardi, L., & Bressan, A. 2008, A&A, 482, 883
Martins, F., Hillier, D. J., Paumard, T., et al. 2008, A&A, 478, 219
Mengel, S., & Tacconi-Garman, L. E. 2007, A&A, 466, 151
Perina, S., Barmby, P., Beasley, M. A., et al. 2009, A&A, 494, 933
Pessev, P. M., Goudfrooij, P., Puzia, T. H., & Chandar, R. 2006, AJ, 132, 781
Pfalzner S. 2009, A&A, 498, L37
Portegies Zwart, S. F., McMillan, S. L. W., & Gieles, M. 2010, ARA&A, 48, 431
Povich, M. S., Churchwell, E., Bieging, J. H., et al. 2009, ApJ, 696, 1278
Sabbi, E., Sirianni, M., & Nota, A. 2008, AJ, 135, 173
Salpeter, E. 1955, ApJ, 121, 161
Smith, C. H., Bourke, T. L., Wright, C. M., et al. 1999, MNRAS, 303, 367
Straizys, V., & Lazauskaitė, R. 2009, Baltic Astron., 18, 19
Vazquez, G. A., & Leitherer, C. 2005, ApJ, 621, 695
Whitworth, A. 1979, MNRAS, 186, 59
Witt, A. N., Thronson, H. A., & Capuano, Jr., J. M. 1992, ApJ, 393, 611
Wolk, S. J., Spitzbart, B. D., Bourke, T. L., & Alves, J. 2006, ApJ, 132, 110
Worthey, G., & Lee H.-C. 2011, ApJS, 193, 1